submitted: *Visual Neuroscience*

A High Frequency Resonance in the Responses of Retinal Ganglion Cells to Rapidly Modulated Stimuli: A Computer Model

Denning, KS [1], George, JS [1], Travis, BJ [2], Theiler, J [3], Marshak, DW [4],

Kenyon, GT [1]

[1] P-21, Biological and Quantum Physics Group, Los Alamos National Laboratory (LANL), Los Alamos, NM
[2] EES-2: Atmospheric Climate & Environmental Dynamics, LANL
[3] NIS-2: Space And Remote Sensing Sciences, LANL
[4] Dept. of Neurobiology and Anatomy, University of Texas Medical School, Houston, TX

To whom correspondence should be addressed:

Garrett Kenyon
P-21, MS D454,
Los Alamos National Laboratory
Los Alamos, NM 87545
phone: 505-667-1900
fax: 505-665-4507
email: gkenyon@lanl.gov

Running title: High Frequency Resonance in Ganglion Cells

manuscript pages: 33
table: 2
figures: 9

key words: synchrony, gamma oscillations, alpha ganglion cell, amacrine cell, gap junction, simulation

Abstract

Brisk ganglion cells in the cat retina exhibit a high frequency resonance (HFR) in their responses to large, rapidly modulated stimuli. We used a computer model of the inner retina to test the hypothesis that negative feedback from axon-bearing amacrine cells could account for the experimentally observed properties of HFRs. Consistent with this hypothesis, temporal modulation transfer functions (tMTFs) recorded from model ganglion cells exhibited HFRs whose amplitudes, peak frequencies and phase shifts were consistent with published data. Because the axon-bearing amacrine cells made diffuse projections over a large area, the HFRs recorded from model ganglion cells became much more prominent as the stimulus size increased, a finding consistent with the observed size dependence of HFRs in the cat retina. We further used the retinal model to explore the relationship between HFRs and high frequency oscillatory potentials (HFOPs), which have likewise been recorded from brisk cell types in the cat retina in response to large, slowly varying stimuli. The frequency, amplitude, and duration recorded from model ganglion cells were similar to experimentally measured values, showing that realistic HFRs and HFOPs can be produced with a single set of model parameters. Changes in the peak frequencies of HFRs and HFOPs were strongly correlated across a range of stimulus sizes and ganglion cell phase response curves and power spectra showed evidence of entrainment near the point where the resonance and oscillation frequencies became similar. These empirical results suggest model-independent strategies for testing the hypothesis that HFRs and HFOPs arise from a common set of physiological mechanisms.

Introduction

A standard measure of a retinal ganglion cell's responsiveness to time varying stimuli is the temporal modulation transfer function (tMTF), which plots the amplitude of the sinusoidal changes in firing rate at the fundamental temporal modulation frequency of a harmonically-varying stimulus. In response to diffuse, temporally modulated gratings, the tMTFs recorded from brisk ganglion cells in the cat retina exhibit a prominent high frequency resonance (HFR) between 60-70 Hz (Frishman et al., 1987). Although HFRs are more pronounced in alpha (Y) cells, they can be detected in beta (X) ganglion cells as well. The physiological mechanisms underlying HFRs have not yet been established, but constraints can be inferred from published data. HFR amplitudes are approximately twice as large in response to diffuse temporally modulated stimuli as for optimal spatial frequency gratings (Frishman et al., 1987). The mechanisms underlying HFRs must therefore extend into the ganglion cell surround, as any mechanism acting wholly within the ganglion cell receptive field center could not account for their observed size dependence. Feedback from horizontal cells onto cone pedicles can produce a resonance peak under some conditions (Smith, 1995). However, the resonance in horizontal cell tMTFs is much smaller and occurs at lower temporal frequencies (Foerster et al., 1977) than the HFRs measured in cat alpha ganglion cells. Anatomical studies have identified a class of amacrine cells in the cat retina that appear well suited to mediate HFRs. These amacrine cells are tracer coupled to alpha ganglion cells and give rise to long axon-like processes (Vaney, 1994). The processes of axon-bearing amacrine cells have been shown to make synaptic contacts onto bipolar, amacrine, and ganglion cells, including alpha ganglion cells (Kolb & Nelson, 1993; Freed et al., 1996), a finding which suggests that the population of axon-bearing amacrine cells tracer coupled to the alpha ganglion cells form a negative feedback loop. Here,

we used a computer model of the inner retina to investigate whether axon-mediated feedback consistent with retinal anatomy could account for the experimentally observed properties of HFRs.

Sharp resonance peaks are typically associated with oscillatory responses, or ringing, at or near the resonance frequency. Consistent with this expectation, it has been known for many decades that large or diffuse stimuli can evoke high frequency oscillatory potentials (HFOPs) in the cat retina ranging from 60-120 Hz (Steinberg, 1966; Laufer & Verzeano, 1967; Neuenschwander & Singer, 1996; Neuenschwander et al., 1999). HFOPs are only evoked only by large spots whose diameter exceeds the width of the ganglion cell receptive field center by several factors (Neuenschwander et al., 1999), demonstrating that both HFRs and HFOPs depend similarly on stimulus size. Previous modeling studies suggest that axon-mediated feedback onto alpha ganglion cells is capable of generating HFOPs that are consistent with experimental data in a manner that is robust to changes in individual model parameters or numerical precision (Kenyon & Marshak, 1998; Kenyon et al., 2003). However, the ability of axon-mediated feedback to simultaneously account for the experimentally observed properties of HFRs has not been explored. An additional goal of the present study was therefore to determine whether both HFRs and HFOPs could be explained by axon-mediated feedback using a single set of model parameters.

In addition to axon-mediated feedback, there are other circuits in the inner retina that also might contribute to HFRs and HFOPs, including amacrine cell feedback onto bipolar cell terminals (Euler & Wassle, 1998; Euler & Masland, 2000; Freed et al., 2003; Shields & Lukasiewicz, 2003) and intrinsic oscillatory kinetics of voltage-gated channels in wide-field amacrine cells (Solessio et al., 2002; Vigh et al., 2003). Although it was not practical to model

all possible feedback loops in the inner retina that might contribute to resonance and/or oscillatory phenomena, we used axon-mediated feedback to investigate empirical relationships between HFRs and HFOPs that might be model-independent. In particular, we used the model to explore relationships between HFRs and HFOPs that seemed likely to result from general properties of cellular and/or synaptic feedback loops and thus might be expected to hold regardless of the specific physiological mechanism, or mechanisms, involved. Another goal of the present study was therefore to identify model-independent experimental strategies that could be used to test the hypothesis that HFRs and HFOPs are different aspects of a single phenomenon arising from a common set of physiological mechanisms.

Methods

Computer Model:

Complete details of the model, its connection to retinal anatomy and physiology, and its robustness to changes in individual parameter values or level of numerical precision, have appeared elsewhere (Kenyon et al., 2003). Only an abbreviated description of the model is presented here. There were 5 distinct cell types in the model: bipolar cells (BPs), small amacrine cells (SAs), large amacrine cells (LAs), poly-axonal amacrine cells (PAs), and alpha ganglion cells (GCs), whose interconnections could be organized into three general categories (fig. 1). All cell types were modeled as single compartment, RC circuit elements obeying a first order differential equation that could be written compactly in terms of matrix multiplications as follows:

$$\dot{\vec{V}}^{(k)} = -\frac{1}{\tau^{(k)}}\left(\vec{V}^{(k)} - \sum_{k'} \vec{W}^{(k,k')} \cdot f^{(k,k')}\left(\vec{V}^{(k')}\right) \cdot \vec{W}^{(k,k')^T} - b^{(k)} - \vec{L}^{(k)} \right), \qquad (1)$$

where $\vec{V}^{(k)}$ are the membrane potentials of cells of type k, $(1 \le k \le 5)$, $\tau^{(k)}$ is the time constant, $b^{(k)}$ is the resting potential, $\vec{L}^{(k)}$ represents light stimulation (to bipolar cells only), $\vec{W}^{(k,k')}$ ($\vec{W}^{(k,k')^T}$) gives the connection strengths between presynaptic, k', and postsynaptic, k, cell types as a function of their vertical (horizontal) separation measured in rows (columns), and the functions $f^{(k,k')}$ are input-output relations, detailed below. To represent a finite reversal potential for inhibitory currents, membrane potentials were not allowed to drop below a minimum value of -2. Axonal conduction velocity was 8 pixels/msec, where the pixel diameter equaled center-to-center distance between neighboring BPs. Axonal synapses had an additional fixed delay of 2 msec. All other synaptic interactions were delayed by 1 msec. The integration

time step was 1 msec, and the dynamical equations were integrated using an explicit Euler method.

The input-output function for gap junctions was given by the identity:

$$f^{(k,k')}\left(\vec{\vec{V}}^{(k')}\right) = \vec{\vec{V}}^{(k')}, \tag{2}$$

where the dependence on the presynaptic potential has been absorbed into the definition of $\tau^{(k)}$. The input-output function for graded synapses was constructed by comparing, on each time step, a random number with a Fermi-function:

$$f^{(k,k')}\left(\vec{\vec{V}}^{(k')}\right) = \theta\left(\left[\frac{1}{1+\exp\left(-\alpha\vec{\vec{V}}^{(k')}\right)}\right] - r\right), \tag{3}$$

where α sets the gain (equal to 4 for all graded synapses), r is a uniform random deviate between 0 and 1, and θ is a step function, $\theta(x) = 1,\ x \geq 0$; $\theta(x) = 0,\ x < 0$.

Finally, the input-output relation used for conventional synapses was:

$$f^{(k,k')}\left(\vec{\vec{V}}^{(k')}\right) = \theta\left(\vec{\vec{V}}^{(k')} - \vec{\vec{T}}^{(k')}\right). \tag{4}$$

where the matrix $\vec{\vec{T}}^{(k')}$ denotes the threshold value for each neuron. For spiking cells, a positive pulse (amplitude = 10.0) was applied after the membrane potential crossed threshold, followed by a negative pulse (amplitude = -10.0) on the next time step. The threshold was incremented by 0.5 following each spike, and then decayed back to zero with the time constant of the cell.

Synaptic strengths fell off as Gaussian functions of the distance between the pre- and post-synaptic cells:

$$W^{(k,k')}_{i^{(k)},j^{(k')}} = z\sqrt{W^{(k,k')}}\exp\left[-\frac{\left\|i^{(k)} - j^{(k')}\right\|^2}{2\sigma^2}\right] \tag{5}$$

where $W_{i^{(k)},j^{(k')}}^{(k,k')}$ is the weight factor from the presynaptic cells of type k' to postsynaptic cells of type k, z is a normalization factor that ensured the total integrated synaptic input equaled $W^{(k,k')}$, σ is the Gaussian radius of the connection measured in pixels, and the quantity $\left\| i^{(k)} - j^{(k')} \right\|$ denotes the distance between the i^{th} and j^{th} pre- and post-synaptic columns, taking into account the wrap around boundary conditions employed to mitigate edge effects. An analogous weight factor described the dependence on row separation. Synapses were non-zero only if the output radius of the presynaptic cell overlapped the input radius of the postsynaptic cell. Except for axonal connections, the input and output radii were the same for all cell types.

The robustness of model has been previously established with respect to variations in single parameter values of up to ±20% and for changes in the integration time step over several orders of magnitude (Kenyon et al., 2003). Values for model parameters that provided a good fit to the HFRs and HFOPs measured experimentally are listed in tables 1 and 2.

Stimuli

The model retina was stimulated by temporally modulated spots of varying size and by drifting gratings covering a range of spatial frequencies. Spot stimuli were used most often as these allowed us to pool over many ganglion cells, thereby greatly improving the signal-to-noise ratio of measured responses. Such pooling was not possible using drifting gratings, as the phase of the coherent oscillations relative to the applied modulation changed as a function of position along the axis of motion. Given computational constraints, it was not feasible to reproduce the long recording times employed in physiological experiments, but this limitation was overcome by simultaneously recording from many ganglion cells in parallel. In all experiments, the modulation amplitude, defined as (peak - trough)/(peak + trough), was equal to 0.5. The

maximum intensity for all temporally modulated stimuli was set to 0.75 and the minimum intensity to 0.25. Each temporally modulated stimulus thus produced a net increase in the time-averaged intensity of 0.5. To further increase the number of stimulated cells available for pooling, multiple spots were typically presented on the same run. To ensure that the interactions between spots were negligible, the density of spots was kept low—in no case did presenting multiple spots cause more than $1/16^{th}$ of the total retinal area to be stimulated. In test cases we verified that equivalent results were obtained when only a single spot stimulus was applied. In order to approximate the dynamics of the outer retina, which was not explicitly modeled, a temporal low pass filter with a time constant of 10 msec was applied to all stimuli.

Data Analysis

Unless otherwise noted, tMTFs were constructed by as described by Frishman et al (1987), except that we used multi-unit as opposed to single-unit measures. Multi-unit peri-stimulus-time-histograms (mPSTHs) were constructed for each temporal modulation frequency. In a typical trial, the simulation was allowed to run without stimulation for 200 msec to eliminate startup artifacts. To allow a quasi-stationary state to be reached, temporally modulated stimuli, in sine phase, were applied for 800 msec before recording data for analysis. Data was always collected for 16 cycles of the sinusoidally varying stimulus, with successive 4 cycle epochs being overlaid (i.e. 4 epochs per trial). Data was binned using a time unit of 4 msec. The mPSTHs were averaged over 10 trials for frequencies below 50 Hz, and over 25 trials for frequencies above 50 Hz. The mPSTHs for each temporal modulation frequency were Fourier transformed to determine the magnitude and phase of the fundamental component. Multi-unit tMTFs were constructed by plotting the magnitude of the fundamental Fourier component as a function of the

temporal modulation frequency. Multi-unit phase response curves were similarly obtained by plotting the phase of the fundamental Fourier component on the same abscissa. Because the phase could only be determined modulo 360 degrees, smoothness criteria were employed to resolve potential ambiguities. When the magnitude and phase of the fundamental Fourier components were computed prior to averaging over stimulus trials, in order to avoid the loss of high frequency periodic structure that was not phase locked to the stimulus, resonance peaks were typically larger. However, results presented here followed the analysis protocol closest to that used by Frishman et al (1987).

For examining HFOPs in response to stationary spots, data was collected between 200-800 msec after stimulus onset, thereby avoiding the transient portion of the response. Multi-unit power spectra were constructed by first binning the spikes of all stimulated cells into a single-trial mPSTH, the set of which were used to compute multi-unit power spectra for each stimulus trial and the results averaged across trials. Multi-unit autocorrelation functions were calculated by computing single-trial autocorrelation functions from the single-trial mPSTHs, and then averaging over trials. Time-dependent multi-unit autocorrelation functions in response to slowly drifting gratings were computed by dividing the single-trial mPSTHs into overlapping time windows, 200 msec long and offset from each other by 50 msec, as described in Neuenschwander et al. (1999).

Results

Multi-unit peri-stimulus-time-histograms (mPSTHs), constructed by binning the spikes of all 16 model ganglion cells activated by a large sinusoidally varying spot (4×4 GCs), exhibited a bimodal dependence on the temporal modulation frequency (fig. 2, histograms). The amplitude of the response to a sinusoidal stimulus was relatively large for a temporal modulation frequency of 14 Hz, greatly reduced at 45 Hz, large again at 67 Hz, and then small again at 87 Hz. To better quantify the responses of the model ganglion cells to large, temporally modulated stimuli, the mPSTHs were Fourier analyzed to determine the amplitude and phase of the firing rate modulations at the fundamental temporal frequency of the stimulus (fig. 2, lines). The amplitudes and phases of the fundamental Fourier components were used to construct a multi-unit tMTF and phase response curve (figs. 3a and 3b, respectively). Corresponding values obtained from cat alpha ganglion cells, re-plotted from Frishman et al (1987), are shown for comparison (see insets).

As with alpha cells in the cat retina, the firing rates of the model ganglion cells could be modulated by temporal frequencies up to approximately 100 Hz. The amplitude of the sinusoidal variations evoked in the retinal model were largest for stimulus frequencies around 14 Hz, slightly above the peak modulation frequency in the cat retina. The responses of ganglion cells to temporally modulated stimuli are complex (Reich et al., 1997), reflecting a combination of intrinsic properties and circuit interactions (Frishman et al., 1987). The responses of cat ganglion cells to direct injections of sinusoidally varying currents exhibit a peak around 10 Hz (Robinson & Chalupa, 1997), suggesting that the broad low-frequency resonance in the tMTF is primarily an intrinsic property of retinal neurons, although phase-shifts between the center and surround may contribute as well (Frishman et al., 1987). Here, our interest is in the

physiological mechanisms underlying the high-frequency resonance at approximately 67 Hz. In both the cat and model data, the high frequency resonance peak in the tMTF was very prominent, with a half width of approximately 20 Hz and a peak-to-baseline ratio of approximately 4. Qualitative features of the experimentally recorded tMTF, especially the high frequency resonance, are well captured by the retinal model.

The phase response curve obtained from the retinal model was also qualitatively similar to that recorded from cat alpha cells (fig. 3b). In both sets of data, responses at moderate temporal modulation frequencies, below 10 Hz, were phase advanced relative to the stimulus. A phase advance between 0-90 degrees is consistent with the transient character of alpha ganglion cell light responses, which peak when the sinusoidal input is varying most rapidly. At very low temporal frequencies, below 2 Hz, model ganglion cell responses moved back into phase with the stimulus, a behavior that was not exhibited by cat alpha cells. This discrepancy may be due to the absence of light adaptation in the retinal model, which introduces an additional phase advance in the responses of cat alpha cells to slowly varying stimuli. As the temporal modulation frequency was increased above 2 Hz, the response phase of the model ganglion cells became progressively more lagged, reflecting a fixed activation latency of approximately 10 msec. In cat alpha cells, the corresponding phase lag accumulated more steeply as a function of temporal frequency than in the retinal model, which lacked an outer retina and thus exhibited shorter response latencies. The trend towards increasing phase lag was interrupted by a kink in the phase response curve that was present in both the experimental and model data. This kink, or phase advance, was roughly aligned with the onset of the HFR peak in the multi-unit tMTF. We interpreted this phase advance as evidence of entrainment, representing the frequency band over

which endogenous oscillations due to inner retinal circuitry first become phase locked to the applied temporal modulation.

Brisk ganglion cells in the cat retina exhibit HFOPs when stimulated by stationary or slowly varying stimuli (Neuenschwander et al., 1999). Using identical parameters, HFOPs similar to those reported in the cat retina could be evoked in the retinal model by slow 2 Hz variations of the same 4×4 stimulus used in constructing the tMTFs shown above. The single-trial mPSTHs were divided into overlapping 200 msec windows, offset by 50 msec from each other, and the time-dependent multi-unit autocorrelogram was computed for each segment and then averaged over trials (fig. 4). The slow temporal modulation due to the stimulus (mPSTH) is plotted along the x-axis, while the conventional time-independent multi-unit autocorrelogram is plotted along the y-axis. HFOPs are clearly revealed by the pronounced periodic structure in the multi-unit correlogram, at a frequency of approximately 70 Hz. Very similar results have been obtained from cat alpha ganglion cells in response to slowly drifting gratings (Neuenschwander et al., 1999). A single set of model parameters was thus able to qualitatively reproduce the basic characteristic of both the HFRs and HFOPs measured in the cat retina.

In recordings from cat ganglion cells, HFRs became much more prominent as the spatial wavelength of the grating stimulus was increased (Frishman et al., 1987). Similar effects were present in the responses of the model ganglion cells as a function of stimulus size (fig. 5). By stimulating a larger area of the model retina, bigger stimuli were able to recruit greater amounts of axon-mediated inhibition, thus amplifying the resonance response of the feedback circuit. Temporally modulated spots covering either 1×1, 2×2, or 8×8 ganglion cells, produced HFRs whose amplitudes increased markedly with stimulus area. The resonance peak produced by the 1×1 spot, which covered only a single ganglion cell, was negligible, showing that intrinsic

properties or synaptic mechanisms restricted to the receptive field center made no contribution to HFRs in the retinal model. The HFR peak was approximately proportional to spot size.

HFOPs recorded from cat ganglion cells become larger with increasing stimulus size (Neuenschwander et al., 1999). A similar size effect was accounted for by the retinal model (fig. 6). Multi-unit power spectra were computed in response to static presentations of different sized spots. A small 1×1 spot, centered over a single ganglion cell, produced a negligible high frequency peak in the multi-unit power spectrum, whereas larger spots produced a very prominent peak around 75 Hz. A spot of intermediate size produced a spectral peak that was intermediate in amplitude between those produced by the small and large spots, showing that like HFRs, HFOPs depend in a continuous fashion on stimulus size.

In the retinal model, the peak frequencies of both HFRs and HFOPs depended on stimulus size as well. Such size dependence indicates that the underlying mechanisms are non-linear, as the frequency of a linear oscillator is independent of the applied stimulus. The shifts in the oscillatory and resonance frequencies predicted by the retinal model are reminiscent of the changes in temporal filtering properties associated with contrast gain control in cat ganglion cells (Shapley & Victor, 1978), which likewise depend on stimulus dimensions as well as contrast (Shapley & Victor, 1979). The similar size dependence exhibited by HFRs and HFOPs suggests a straightforward experimental strategy for testing the hypothesis that both phenomena share a common underlying mechanism. As the stimulus dimensions are varied, changes in the peak frequency of HFRs should be correlated with changes in the peak frequency of HFOPs. We used the retinal model to estimate the expected result of such an analysis (fig. 7). For a range of stimulus sizes, the peak oscillatory and resonance frequencies, determined by fitting it with a Lorentzian, were plotted against each other (fig. 7). Data from both spots and gratings, indicated

by circles and squares, were used for this analysis. The HFOP and HFR peak frequencies were strongly correlated across the stimulus set. The slope of the best-fit line was different from one, probably due to non-linearities in the underlying mechanism, but a strong relationship between the two frequencies was nonetheless clear. Our results thus illustrate a straightforward experimental strategy for testing the hypothesis that HFRs and HFOPs are related phenomena arising from a common set of physiological mechanisms.

For slowly varying stimuli, the evoked responses exhibit two characteristic frequencies, a slow modulation locked to the stimulus and a fast modulation corresponding to the intrinsic oscillation frequency of the axon-mediated feedback loop. As the rate of stimulus variation is increased, however, there must come a point where the two oscillations can no longer remain independent of each other. The intrinsic oscillation will become locked to the external modulation of the stimulus. This entrainment of the intrinsic oscillation to the external stimulus is predicted to have at least three experimentally observable consequences. 1) As already shown, the phase response curve will show an abrupt advance as the faster intrinsic rhythm is captured by the slower modulation of the external stimulus. 2) The multi-unit power spectra will exhibit two primary peaks (plus harmonics) at temporal modulation frequencies that are well below or well above the resonance/oscillation frequency, but only a single primary peak around the resonance/oscillation frequency. 3) In response to a drifting grating, the response phase relative to the stimulus will exhibit a complex dependence on the position of the recorded cell relative to the axis of motion. We used the retinal model to explore these latter two predicted effects.

To examine the response at frequencies other than the fundamental, the full power spectra were computed for a range of temporal modulation frequencies using the same 4×4 stimulus employed in figures 2-4. All power spectra exhibited primary peaks at the fundamental

temporal modulation frequency (fig. 8, arrows). At temporal modulation frequencies well below the resonance/oscillation frequency, a secondary primary peak, due to the intrinsic oscillations of the retinal network, was evident at approximately 67 Hz. As the temporal modulation frequency neared the resonance/oscillation frequency, however, the two spectral peaks collapsed into a single peak, consistent with the hypothesis that the external modulation had entrained the endogenous network oscillations. At temporal modulation frequencies well above the resonance/oscillation frequency, there were again two peaks in the power spectra, showing that the two processes were no longer entrained.

In the cat retina, HFOPs are coherent across contiguous stimuli (Neuenschwander & Singer, 1996; Neuenschwander et al., 1999), such that all neurons activated by the stimulus oscillate at the same frequency and phase. Such coherence was implicit in our method of analysis, in which the spike trains of all stimulated cells were combined into a single multi-unit measure. Indeed, non-coherent oscillations would not have been detected by our procedure. The strong phase locking between cells produced by HFOPs poses a potential paradox, however, when we consider the responses to rapidly drifting gratings. At low temporal modulation frequencies, ganglion cell responses can be phase locked both to the stimulus and to each other, as very different time scales are involved. As the external temporal modulation frequency approaches the intrinsic oscillation frequency of the network, however, it is no longer possible to remain phase locked to both the internally and externally generated rhythms simultaneously. To study this question, we plotted the response phase, relative to the local stimulus phase, as a function of position along a diffuse drifting grating (fig. 9). At low temporal modulation frequencies, all cells responded at the same phase relative to the stimulus, regardless of their position along the axis of motion. At temporal modulation frequencies near resonance, however,

the response phase become dependent on the cell's position along the axis of motion. Since entrainment requires there be only a single oscillation frequency, which must in turn be coherent across all cells responding to the same cycle of the stimulus, it follows that the phase of any given neuron's response will depend on its position relative to the edge of the grating.

Discussion

In the cat retina, alpha ganglion cells exhibit prominent HFRs in their responses to long wavelength gratings (Frishman et al., 1987). We developed a computational model to investigate whether feedback circuitry consistent with retinal anatomy could account for this observation. Computational models are useful for connecting anatomy to physiology, as they can address the question of whether a given set of mechanisms is sufficient to account for a given behavior. The present study was strongly motivated by retinal anatomy. Patterns of tracer coupling indicate that alpha ganglion cells in the cat retina are electrically coupled to a population of amacrine cells with wide axonal fields extending out to several millimeters (Vaney, 1994). In our model, the axon-bearing amacrine cells received a major fraction of their excitatory input via gap junctions with neighboring alpha ganglion cells, and in turn makes strong inhibitory synapses onto the surrounding neurons, including ganglion cells, bipolar cells, and other amacrine cells. Our results indicate that this axon-mediated feedback loop forms a naturally resonant circuit that reproduces the main experimental properties of HFRs measured in cat ganglion cells.

Time varying stimuli, if modulated at the correct temporal frequency, can tap into the resonance circuit created by the axon-mediated feedback loop. Ganglion cells, activated during the rising or positive phase of a sinusoidal stimulus, will in turn activate axon-bearing amacrine cells via gap junctions. At resonance, the axon-bearing amacrine cells give rise to delayed inhibition that does not arrive until after the peak portion of the stimulus has passed, during the declining or negative phase of the stimulus where it serves merely to further depress ganglion cell responses. By the time the next rising or positive phase of the stimulus cycle begins, the

axon-mediated inhibition will have terminated, thus potentiating, via disinhibition, the positive portion of the ganglion cell response.

Multi-unit tMTFs generated by the retinal model exhibited resonance peaks that were qualitatively similar to the HFRs observed experimentally. Employing spot stimuli of varying sizes, the HFRs recorded from the model ganglion cells spanned a range of amplitudes and frequencies that overlapped those of experimentally measured HFRs. In cat alpha cells, HFR peaks produced by diffuse sinusoidal gratings were approximate half the amplitude of the much broader resonance peaks present at low temporal modulation frequencies. The relative amplitudes of the low and high frequency resonance peaks in the retinal model depended on the size of the time varying stimulus. Small spots produced negligible HFRs while big spots produced large HFRs, the largest of which matched or exceeded the height of the low frequency resonance peak. Such large HFRs have not been recorded experimentally, but tMTFs have only been evaluated at high temporal modulation frequencies for a limited range of stimuli. The retinal model also accounted for the high frequency kink in the phase response curve recorded from cat alpha cells, which was due to entrainment of the intrinsic network oscillation by the external time-varying stimulus. In general, the responsiveness of the retinal model to temporally modulated stimuli was less than that of cat alpha ganglion cells. This may, in part, reflect the absence of starburst amacrine cells in the model, which in the cat co-stratify with alpha cells (Vardi et al., 1989) and respond robustly to temporally varying stimuli (O'Malley & Masland, 1993). Nevertheless, the qualitative features of experimentally measured HFRs were well accounted for by the retinal model.

Cat ganglion cells have been shown to generate robust HFOPs in response to large stimuli over a similar range of frequencies (Neuenschwander et al., 1999). A computer model

was used to test the hypothesis that both HFRs and HFOPs could arise from the same retinal circuitry. Our results support this hypothesis, as a semi-realistic model of axon-mediated feedback in the inner retina was able to reproduce both phenomena. In particular, the model also accounted for the main experimentally observed characteristics of HFOPs, particularly their frequency and size dependence. HFOPs in cat retinal ganglion cells have been shown to extend over a range of frequencies, from as low as 30 Hz during spontaneous activity, to between 60-110 Hz in response to large, high contrast stimuli. In comparison, HFRs so far described have been restricted to a relatively narrow frequency band, between 60-70 Hz. However, HFRs have so far only been presented for a single alpha ganglion cell using temporally modulated gratings, while experiments investigating HFOPs have employed a much broader range of stimuli and include data from many cells. Our results predict that the resonance frequency of HFRs will also depend on stimulus parameters, particularly size, and will cover a dynamic range similar to that encompassed by HFOPs. Indeed, a key experimental test of the hypothesis that HFRs and HFOPs arise from a common feedback mechanism is that the shifts in the resonance and oscillatory frequencies arising from changes in stimulus parameters will be strongly correlated.

We used the retinal model to identify additional experimental strategies that might be used to test the hypothesis that HFRs and HFOPs arise from a common set of physiological mechanisms. Both experiments were motivated by the idea that for temporal modulation frequencies well below resonance, HFOPs should simply ride on top of the sinusoidal variations due to the external stimulus. At temporal modulation frequencies approaching the resonance/oscillations frequency, however, there should be only a single oscillation that is locked to the external stimulus. In the first experiment, we used the retinal model to show how the two

primary peaks present in the single-trial power spectra at low temporal modulation frequencies merged into a single peak near the resonance frequency. In the second experiment, we investigated how entrainment would affect the response phase to a drifting grating along the axis of motion. A spatially distributed group of cells oscillating coherently cannot all respond at the same phase to a drifting grating. Again, using the retinal model, we found that for low temporal modulation frequencies, the response phase was independent of position, but this was no longer true near resonance. Although derived from a specific model based on axon-mediated feedback, the dynamical principles underlying the above predictions appear to be quite general and thus we expect them to hold for a wide range of feedback mechanisms potentially contributing to resonance/oscillatory phenomena in the inner retina. In particular, the above predictions suggest a general, model-independent strategy for testing the hypothesis that HFRs and HFOPs arise from the same cellular and synaptic feedback loops in the inner retina and are in fact different aspects of a single phenomenon.

Beta cells in the cat retina also exhibit HFRs in response to diffuse, temporally modulated gratings, but the resonance is less pronounced than in alpha cells. Such differences between the resonance peaks of alpha and beta cells can be explained within the context of the retinal model by making several reasonable assumptions. First, the longer time constants of beta cells relative to alpha cells (O'Brien et al., 2002) suggests they would be less responsive to high frequency oscillatory input. Second, beta cells are more diffusely stratified than alpha cells (Saito, 1983), and may therefore receive less axon-mediated feedback. Third, unlike alpha cells, beta cells do not make gap junctions with amacrine cells (Vaney, 1994), which may further reduce their HFRs. The smaller size of the beta cells (Boycott & Wässle, 1974; Wässle et al., 1983) would furthermore reduce the amplitude of their HFRs to optimal wavelength gratings.

Given the strong similarities between alpha cells in the cat and M cells in the primate (Peichl, 1991), especially the similarities in their patterns of tracer coupling to axon-bearing amacrine cells (Dacey & Brace, 1992; Vaney, 1994; Jacoby et al., 1996), axon-mediated feedback may be present in the primate retina as well. The tMTFs recorded from peripheral M cells in response to large time varying stimuli exhibit HFRs similar to those seen in the cat retina (Solomon et al., 2002). In addition, small HFRs are evident in the responses of P ganglion cells to luminance gratings (Martin et al., 2001) and an oscillation of approximately 75 Hz is seen in the impulse response of M ganglion cells to large, high contrast stimuli (Lee et al., 1994). More significantly, HFOPs are clearly present in primate (Frishman et al., 2000) and human (De Carli et al., 2001) ERGs. The conclusions of the present study may therefore be relevant to understanding resonance/oscillatory phenomena in the primate retina. HFOPs have been recorded from retinal ganglion cells in many other vertebrate species as well, including frog (Ishikane et al., 1999), mudpuppy (Wachtmeister & Dowling, 1978) and rabbit (Ariel et al., 1983).

The rabbit retina in particular provides a preparation in which predictions of the above model could readily be tested. OFF alpha cells in the rabbit retina are tracer coupled to wide-field amacrine cells but ON alpha cells are not (Hu & Bloomfield, 2003). If coupling between ganglion cells via wide-field amacrine is essential for resonance/oscillatory phenomena, then our model predicts that HFRs should only be present in the tMTFs of OFF alpha cells, and not in the tMTFs of ON alpha cells. On the other hand, HRFs that were present in both ON and OFF rabbit alpha cells under conditions in which only the OFF alpha cells were tracer coupled to wide-field amacrine cells would have to be produce by feedback mechanisms different than those employed in the present model.

Table 1: Cellular parameters.

	τ	b	n×n	d	σ
BP	10.0	-0.0	64×64	0.25	0.25
SA	25.0	-0.5	64×64	0.25	0.25
LA	20.0	-0.25	32×32	1.0	0.5
PA	7.5	-0.025	64×64	0.25/9.0[a]	0.25/3.0[a]
αGC	5.0	-0.025	32×32	1.0	0.5

Explanation of symbols: τ: time constant (msec); b: bias; n×n: array size; d: cutoff radius, σ: Gaussian radius (see eq. 5). [a]Inner radius/outer radius.

Table 2: Synaptic weights.

	BP	SA	LA	PA	GC
BP	*	-0.375[b]	3.0b	-3.0b/-15.0c	*
SA	3.0[b]	*	-3.0[b]	0.0b/-15.0[c]	*
LA	3.0[b]	*	0.25[a]	-3.0a/-15.0[c]	*
PA	0.75[b]	-0.75b	0.25[a]	0.25a/-45.0[c]	0.25[a,d]
GC	9.0[b]	-4.5b	-4.5[b]	0.25[a]/-120.0[c]	*

Each term represents the total integrated weight from all synapses arising from the corresponding presynaptic type (columns) to each cell of the corresponding postsynaptic type (rows), (the quantity $W^{(k,k')}$ in eq. 5). Asterisk (*) indicates absence of corresponding connection. Synapse type indicated by superscript: [a]gap junction, [b]non-spiking synapse, [c]spiking synapse. [d]Maximum coupling efficiency (ratio of post- to pre-synaptic depolarization) for this gap junction synapse: DC=11.3%, Action Potential=2.7%.

Figure Captions

Fig. 1. The model contained five cells types: bipolar (BP) cells, small (SA), large (LA) and poly-axonal (PA) amacrine cells, and alpha ganglion (GC) cells, arranged as a 32x32 square mosaic with wrap-around boundary conditions. Conceptually, connections could be organized into 3 categories. a) Feedforward and feedback inhibition. Excitatory synapses from BPs were balanced by a combination of reciprocal synapses and direct inhibition of the GCs, mediated by the non-spiking amacrine cell types. b) Serial inhibition. The three amacrine cell types regulated each other through a negative feedback loop. c) Resonance circuit. The PAs were excited locally via electrical synapses with GCs and their axons gave rise to widely distributed inhibition that contacted all cell types, but most strongly the GCs and other PAs. Note: not all connections are shown. Explanation of symbols: Excitation (triangles), inhibition (circles), gap junctions (resistors).

Fig. 2. PSTHs due to temporally modulated stimuli. Multi-unit PSTHs (histograms), obtained by averaging the responses of all model GCs activated by a uniform 4×4 spot, binned relative to the phase of the applied sinusoid modulation. Temporal modulation frequencies are shown at the top of each plot. Large sinusoidal modulation was evident at both low and high frequencies. Contrast (peak-trough/average intensity) was 50%. The amplitude and phase of the fundamental Fourier component is shown superimposed (lines).

Fig. 3. HFRs of model and cat alpha ganglion cells. Same stimulus as in figure 2. a) Temporal modulation transfer functions (tMTFs). The multi-unit tMTF recorded from model ganglion

cells, obtained by plotting the magnitude of the fundamental Fourier component as a function of temporal modulation frequency. The maximum response occurred at a broad low frequency resonance between 10-20 Hz, but there was also a prominent high frequency resonance around 70 Hz. Inset: Similar features were present in the tMTF recorded from a cat alpha ganglion cell in response to a diffuse grating. b) Phase response curves. The response phase of the model ganglion cell plotted as a function of temporal modulation frequency. A prominent kink is evident in the phase response curve at frequencies near the rising phase of the HFR peak. Inset: The phase response cure of the cat alpha cell shows qualitatively similar behavior. Experimental data re-plotted from Frishman et al. (1987)

Fig. 4. HFOPs of model ganglion cells in response to slowly varying stimuli. The time-dependent, multi-unit autocorrelogram recorded in response to the same spot stimulus used in figures 2 and 3 modulated at a temporal frequency 1 Hz. The time-dependent autocorrelogram was calculated from the single-trial, multi-unit PSTHs in overlapping 200 msec windows spaced 50 msec apart, and then averaged over trials. Darker intensities represent stronger correlations. The curve along the x-axis gives the sum of the time-dependent autocorrelogram over all correlation delays, which yields the multi-unit PSTH normalized relative to the average firing rate. The curve along the y-axis gives the sum of the time-dependent autocorrelogram over all times during the stimulus, yielding the time-independent autocorrelogram expressed as a fraction of the baseline level. Time relative to the stimulus is plotted along the x-axis, while the correlation delay is plotted along the y-axis. HFOPs are clearly exhibited by the periodic structure along the y-axis, which is in turn modulated by the slowly varying stimulus.

Fig. 5. HFRs increase with stimulus size. The tMTFs of the model alpha cells were computed in response to sinusoidally modulated spots of varying size. Resonance peaks become larger and the resonance frequency changes with increasing spot size. The legend shows the stimulus dimensions of the corresponding curves in units of GC-GC center-to-center distance.

Fig. 6. HFOPs increase with stimulus size. Multi-unit power spectra, normalized by dividing each frequency band by the amplitude of the zero frequency band, computed from single trial ganglion cell responses during maintained spot stimulation. HFOPs, indicated by a pronounced peak in the upper gamma band (60-120 Hz), become larger and shift in frequency as spot size increases.

Fig. 7. The resonance response to temporally modulated spots of various sizes and the HFOPs evoked by maintained application of the same stimuli are linearly related. A plot of the peak resonance frequency vs. peak HFOP frequency shows that the two quantities covary strongly, indicating a common underlying synaptic mechanism.

Fig. 8. Evidence of entrainment in multi-unit power spectra. For temporal modulation frequencies away from the resonance/oscillation frequency, power spectra exhibit two peaks, one corresponding to the driving frequency of the stimulus (arrows) and the other to the natural oscillation frequency of the retinal network. Near the resonance/oscillation frequency, however, only a single spectral peak is present. The collapse of the two spectral peaks into a single peak is evidence of entrainment around the resonance/oscillation frequency.

Fig. 9. Response phase is strongly dependent on cell location at temporal modulation frequencies near the resonance/oscillation frequency. Response phase, relative to the phase of the stimulus, is plotted as a function of cell location relative to the trailing edge of the drifting grating for several different temporal modulation frequencies. a) Below resonance. The phase is approximately independent of position. b) Near resonance. The phase changes rapidly across the grating, due to strong entrainment of HFOPs by the external stimulus. c) Above resonance. The phase is again nearly independent of position.

References

Ariel, M., Daw, N.W. & Rader, R.K. (1983). Rhythmicity in rabbit retinal ganglion cell responses. Vision Research 23(12): 1485-93.

Boycott, B.B. & Wässle, H. (1974). The morphological types of ganglion cells of the domestic cat's retina. Journal of Physiology 240(2): 397-419.

Dacey, D.M. & Brace, S. (1992). A coupled network for parasol but not midget ganglion cells in the primate retina. Visual Neuroscience 9(3-4): 279-90.

De Carli, F., Narici, L., Canovaro, P., Carozzo, S., Agazzi, E. & Sannita, W.G. (2001). Stimulus- and frequency-specific oscillatory mass responses to visual stimulation in man. Clin Electroencephalogr 32(3): 145-51.

Euler, T. & Masland, R.H. (2000). Light-evoked responses of bipolar cells in a mammalian retina. J Neurophysiol 83(4): 1817-29.

Euler, T. & Wassle, H. (1998). Different contributions of GABAA and GABAC receptors to rod and cone bipolar cells in a rat retinal slice preparation. J Neurophysiol 79(3): 1384-95.

Foerster, M.H., van de Grind, W.A. & Grusser, O.J. (1977). The response of cat horizontal cells to flicker stimuli of different area, intensity and frequency. Experimental Brain Research 29(3-4): 367-85.

Freed, M.A., Pflug, R., Kolb, H. & Nelson, R. (1996). ON-OFF amacrine cells in cat retina. Journal of Comparative Neurology 364(3): 556-566.

Freed, M.A., Smith, R.G. & Sterling, P. (2003). Timing of quantal release from the retinal bipolar terminal is regulated by a feedback circuit. Neuron 38(1): 89-101.

Frishman, L.J., Freeman, A.W., Troy, J.B., Schweitzer-Tong, D.E. & Enroth-Cugell, C. (1987). Spatiotemporal frequency responses of cat retinal ganglion cells. Journal of General Physiology 89(4): 599-628.

Frishman, L.J., Saszik, S., Harwerth, R.S., Viswanathan, S., Li, Y., Smith, E.L., 3rd, Robson, J.G. & Barnes, G. (2000). Effects of experimental glaucoma in macaques on the multifocal ERG. Multifocal ERG in laser-induced glaucoma. Doc Ophthalmol 100(2-3): 231-51.

Hu, E.H. & Bloomfield, S.A. (2003). Gap junctional coupling underlies the short-latency spike synchrony of retinal alpha ganglion cells. J Neurosci 23(17): 6768-77.

Ishikane, H., Kawana, A. & Tachibana, M. (1999). Short- and long-range synchronous activities in dimming detectors of the frog retina. Vis Neurosci 16(6): 1001-14.

Jacoby, R., Stafford, D., Kouyama, N. & Marshak, D. (1996). Synaptic inputs to ON parasol ganglion cells in the primate retina. Journal of Neuroscience 16(24): 8041-56.

Kenyon, G.T. & Marshak, D.W. (1998). Gap junctions with amacrine cells provide a feedback pathway for ganglion cells within the retina. Proc R Soc Lond B Biol Sci 265(1399): 919-25.

Kenyon, G.T., Moore, B., Jeffs, J., Denning, K.S., Stephens, G.S., Travis, B.J., George, J.S., Theiler, J. & Marshak, D.W. (2003). A model of high frequency oscillatory potentials in retinal ganglion cells. Visual Neuroscience (in press).

Kolb, H. & Nelson, R. (1993). OFF-alpha and OFF-beta ganglion cells in cat retina: II. Neural circuitry as revealed by electron microscopy of HRP stains. Journal of Comparative Neurology 329(1): 85-110.

Laufer, M. & Verzeano, M. (1967). Periodic activity in the visual system of the cat. Vision Res 7(3): 215-29.

Lee, B.B., Pokorny, J., Smith, V.C. & Kremers, J. (1994). Responses to pulses and sinusoids in macaque ganglion cells. Vision Research 34(23): 3081-96.

Martin, P.R., Lee, B.B., White, A.J., Solomon, S.G. & Ruttiger, L. (2001). Chromatic sensitivity of ganglion cells in the peripheral primate retina. Nature 410(6831): 933-6.

Neuenschwander, S., Castelo-Branco, M. & Singer, W. (1999). Synchronous oscillations in the cat retina. Vision Res 39(15): 2485-97.

Neuenschwander, S. & Singer, W. (1996). Long-range synchronization of oscillatory light responses in the cat retina and lateral geniculate nucleus. Nature 379(6567): 728-32.

O'Malley, D.M. & Masland, R.H. (1993). Responses of the starburst amacrine cells to moving stimuli. J Neurophysiol 69(3): 730-8.

O'Brien, B.J., Isayama, T., Richardson, R. & Berson, D.M. (2002). Intrinsic physiological properties of cat retinal ganglion cells. J Physiol 538(Pt 3): 787-802.

Peichl, L. (1991). Alpha ganglion cells in mammalian retinae: common properties, species differences, and some comments on other ganglion cells. Visual Neuroscience 7(1-2): 155-69.

Reich, D.S., Victor, J.D., Knight, B.W., Ozaki, T. & Kaplan, E. (1997). Response variability and timing precision of neuronal spike trains in vivo. J Neurophysiol 77(5): 2836-41.

Robinson, D.W. & Chalupa, L.M. (1997). The intrinsic temporal properties of alpha and beta retinal ganglion cells are equivalent. Curr Biol 7(6): 366-74.

Saito, H.A. (1983). Morphology of physiologically identified X-, Y-, and W-type retinal ganglion cells of the cat. J Comp Neurol 221(3): 279-88.

Shapley, R.M. & Victor, J.D. (1978). The effect of contrast on the transfer properties of cat retinal ganglion cells. Journal of Physiology 285: 275-98.

Shapley, R.M. & Victor, J.D. (1979). Nonlinear spatial summation and the contrast gain control of cat retinal ganglion cells. Journal of Physiology 290(2): 141-61.

Shields, C.R. & Lukasiewicz, P.D. (2003). Spike-Dependent GABA Inputs to Bipolar Cell Axon Terminals Contribute to Lateral Inhibition of Retinal Ganglion Cells. J Neurophysiol 89(5): 2449-58.

Smith, R.G. (1995). Simulation of an anatomically defined local circuit: the cone-horizontal cell network in cat retina. Visual Neuroscience 12(3): 545-61.

Solessio, E., Vigh, J., Cuenca, N., Rapp, K. & Lasater, E.M. (2002). Membrane properties of an unusual intrinsically oscillating, wide-field teleost retinal amacrine cell. J Physiol 544(Pt 3): 831-47.

Solomon, S.G., Martin, P.R., White, A.J., Ruttiger, L. & Lee, B.B. (2002). Modulation sensitivity of ganglion cells in peripheral retina of macaque. Vision Res 42(27): 2893-8.

Steinberg, R.H. (1966). Oscillatory activity in the optic tract of cat and light adaptation. J Neurophysiol 29(2): 139-56.

Vaney, D.I. (1994). Patterns of neuronal coupling in the retina. Progress in Retinal and Eye Research 13: 301-355.

Vardi, N., Masarachia, P.J. & Sterling, P. (1989). Structure of the starburst amacrine network in the cat retina and its association with alpha ganglion cells. Journal of Comparative Neurology 288(4): 601-11.

Vigh, J., Solessio, E., Morgans, C.W. & Lasater, E.M. (2003). Ionic Mechanisms Mediating Oscillatory Membrane Potentials in Wide-field Retinal Amacrine Cells. J Neurophysiol 20: 20.

Wachtmeister, L. & Dowling, J.E. (1978). The oscillatory potentials of the mudpuppy retina. Invest Ophthalmol Vis Sci 17(12): 1176-88.

Wässle, H., Peichl, L. & Boycott, B.B. (1983). Mosaics and territories of cat retinal ganglion cells. Progress in Brain Research 58: 183-90.

A. Feedforward & Feedback Inhibition

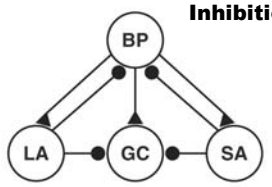

B. Serial Inhibition

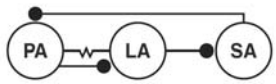

C. Resonance Circuit

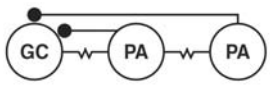

Figure 1

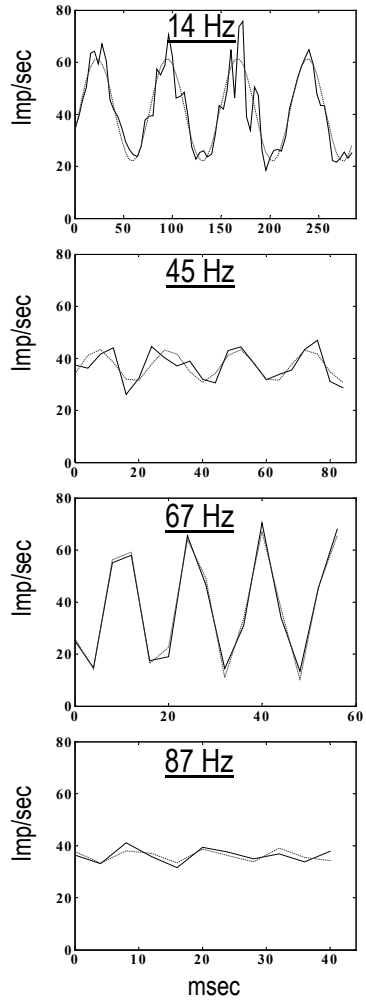

Figure 2

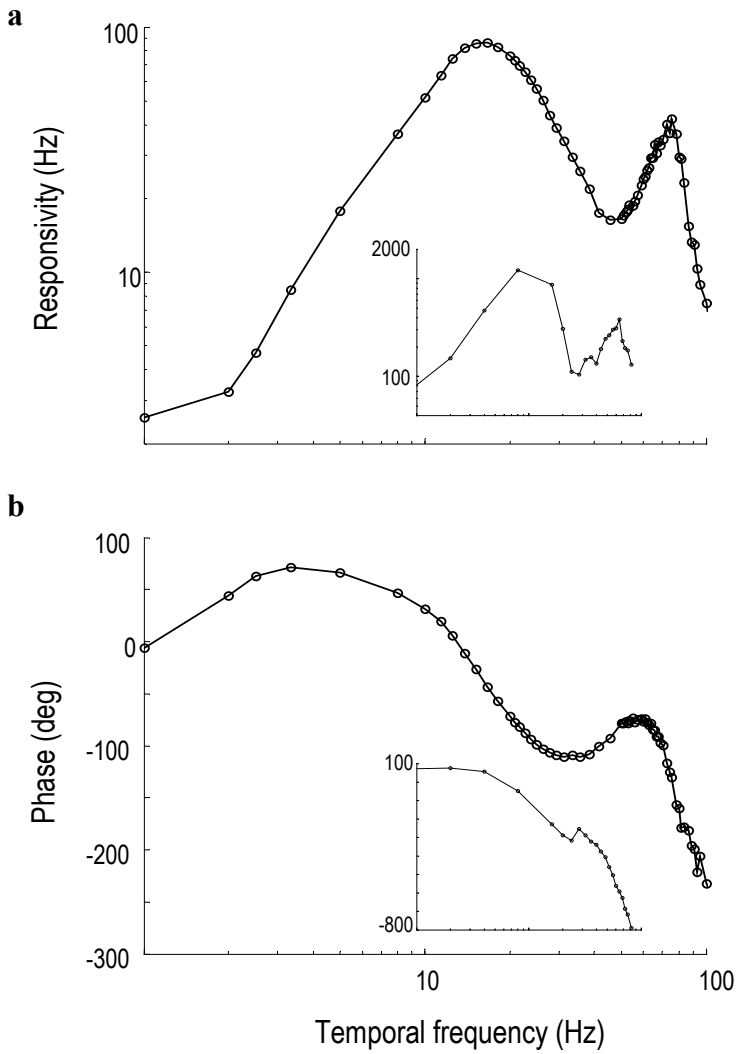
a
100
10
Responsivity (Hz)
2000
100
b
100
0
-100
-200
-300
Phase (deg)
100
-800
10
100
Temporal frequency (Hz)

Figure 3

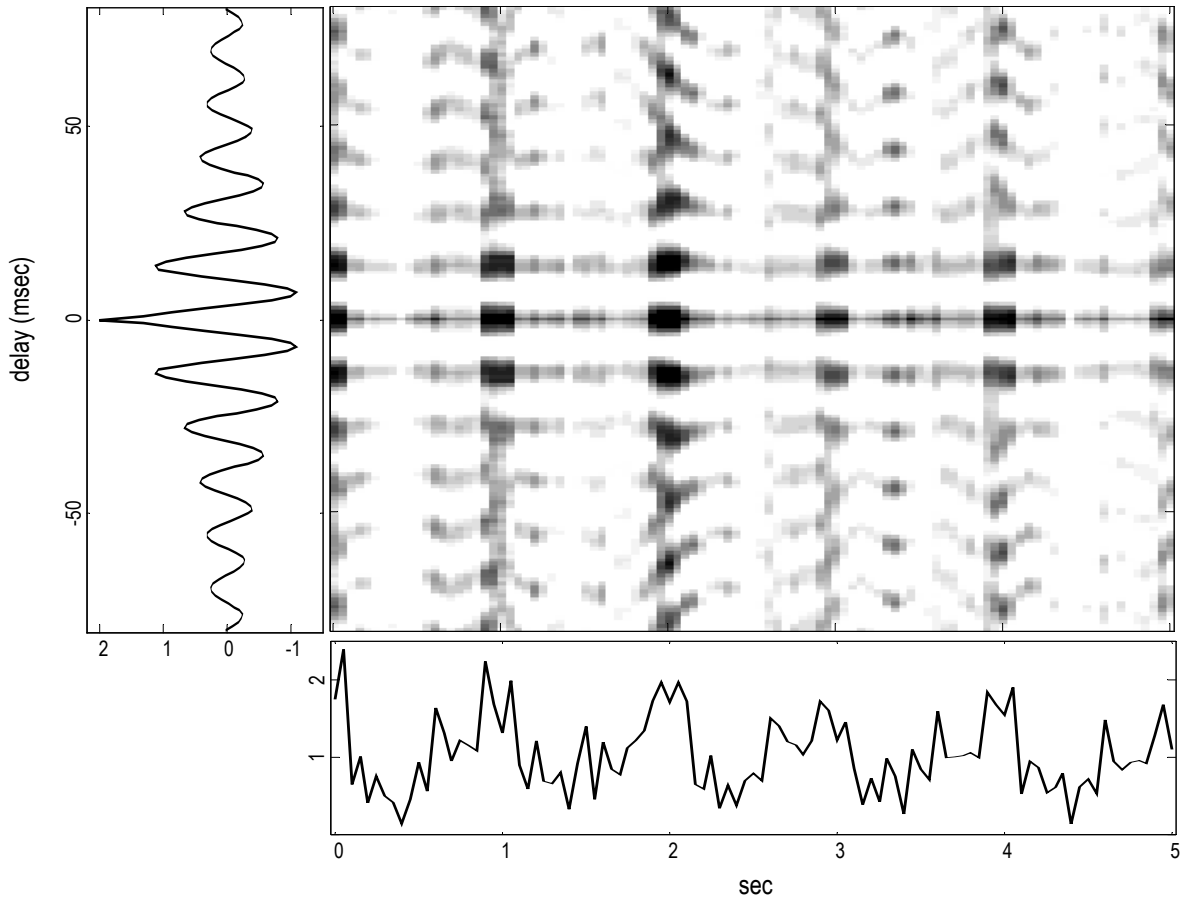

Figure 4

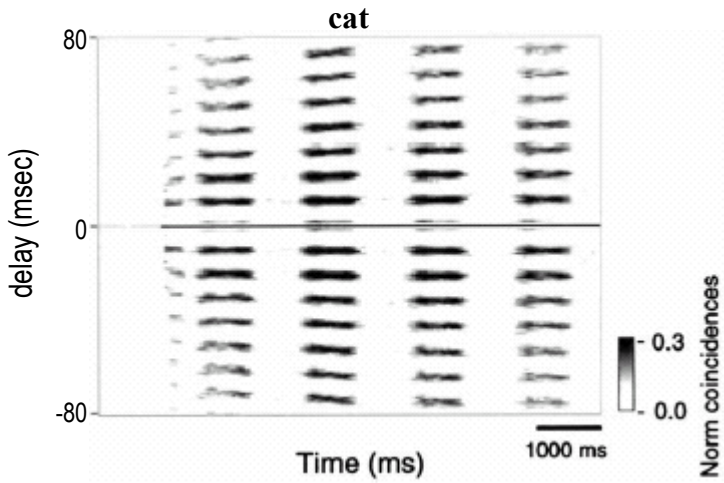

Comparison for figure 4 (reprinted from Neuenschwander and Singer, 1999, for reviewer convenience)

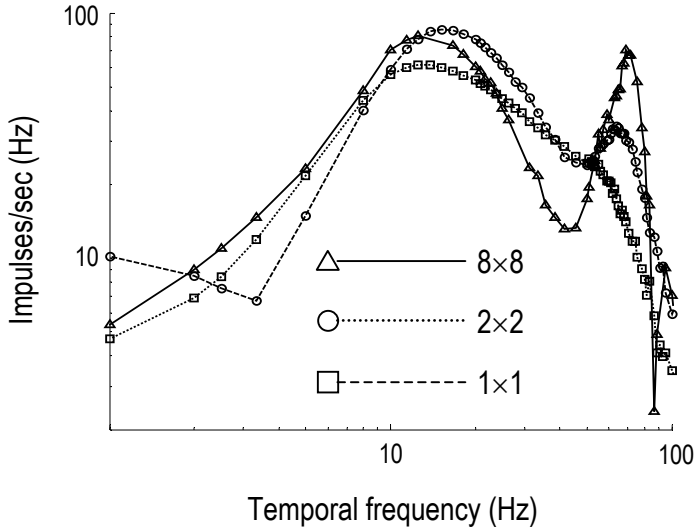

Figure 5

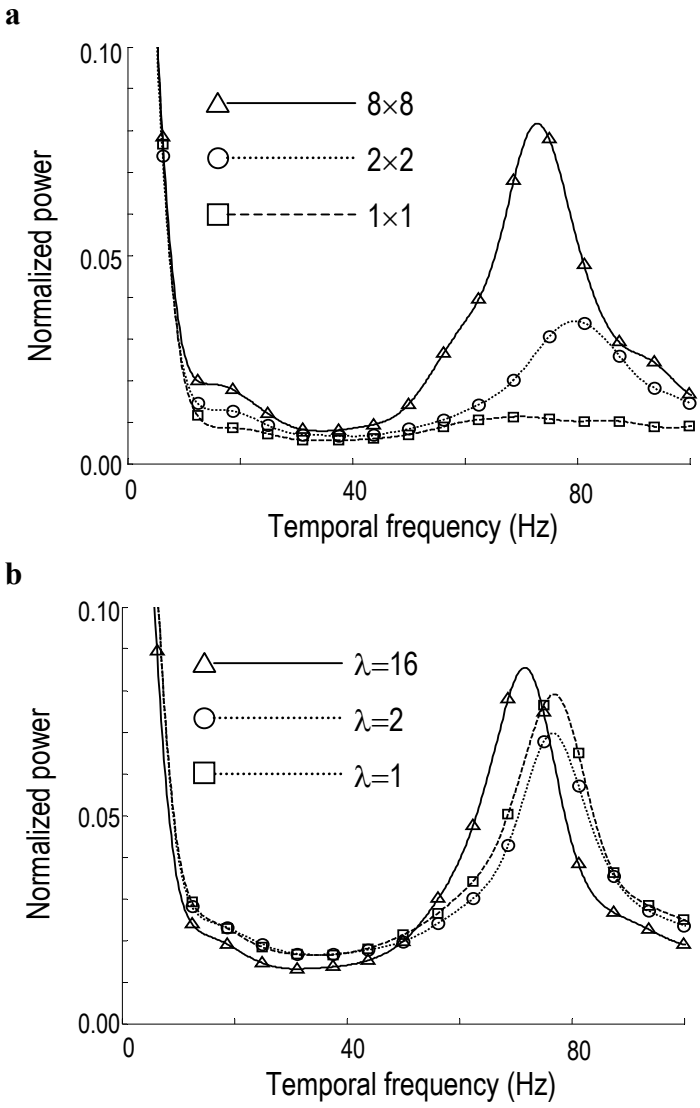
a
0.10
0.05
0.00
Normalized power
8×8
2×2
1×1
0
40
80
Temporal frequency (Hz)
b
0.10
0.05
0.00
Normalized power
λ=16
λ=2
λ=1
0
40
80
Temporal frequency (Hz)

Figure 6

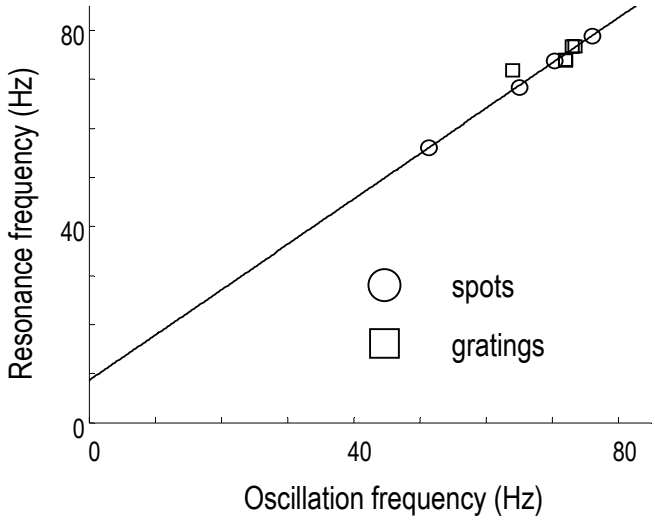
Resonance frequency (Hz)
80
40
0
0
40
80
Oscillation frequency (Hz)
spots
gratings

Figure 7

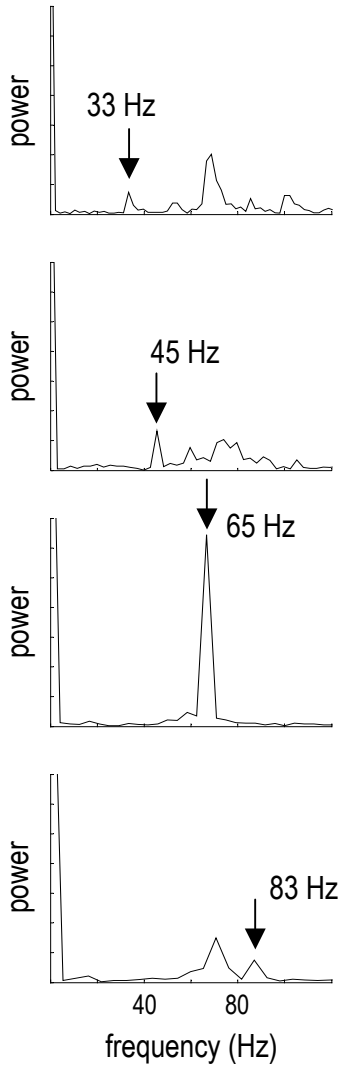
power
33 Hz
power
45 Hz
65 Hz
power
power
83 Hz
40
80
frequency (Hz)

Figure 8

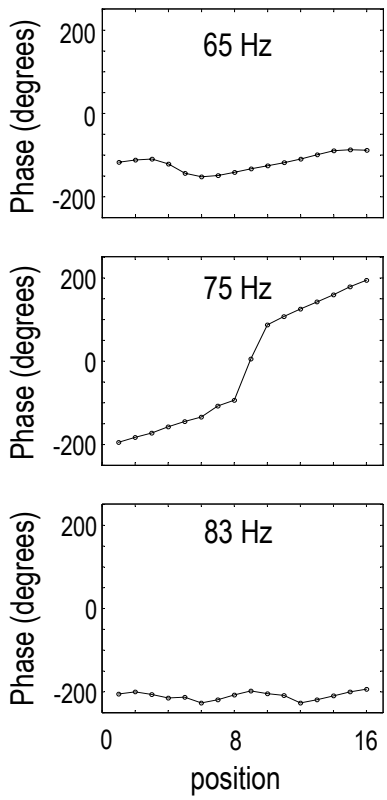

Figure 9